Coaggregation of DISC1 and mutant huntingtin dysregulates PDE4 in Huntington's disease

by

Motomasa Tanaka[1,#,*], Koko Ishizuka[2,#], Yoko Nekooki-Machida[1,#], Ryo Endo[1], Hideyuki Sasaki[3], Noriko Takashima[1], Yusuke Komi[1], Amy Gathercole[4], Elaine Huston[4], Masaru Kurosawa[5], Sun-Hong Kim[2], Nobuyuki Nukina[5], Eiki Takimoto[3], Miles D. Houslay[6], and Akira Sawa[2,*]

Laboratory for [1]Protein Conformation Diseases and [5]Structural Neuropathology, RIKEN Brain Science Institute, Japan; [2]Department of Psychiatry, [3]Division of Cardiology Johns Hopkins University School of Medicine, USA; [4]Institute for Psychology and Neurosciences, University of Glasgow, Glasgow, Scotland, UK;

[6]Institute of Pharmaceutical Sciences, King's College London, London, UK

#, These three authors contributed equally to this work

*Correspondence authors:

Akira Sawa (contact person), asawa1@jhmi.edu;

Motomasa Tanaka, motomasa@brain.riken.jp

The authors have declared that no conflict of interest exists.

Abstract

Huntington's disease (HD) is a representative polyglutamine (polyQ) disease caused by aberrant expansion of the polyQ tract in Huntingtin (Htt). While motor impairment mediated by polyQ-expanded Htt has been intensively studied, molecular mechanisms for non-motor symptoms such as psychiatric manifestations in HD remain elusive. Here we demonstrate that Htt forms a ternary protein complex with DISC1 and cAMP-degrading phosphodiesterase-4 (PDE4), which regulates PDE4 activity. The pathogenic sequestration of amyloidogenic DISC1 into mutant Htt aggregates by cross-seeding is observed in the brains of HD patients and those of the R6/2 model that represents the polyQ pathology of HD. Consequently, the R6/2 model shows a PDE4 fraction becoming out of physiological control by DISC1, aberrantly increasing the activity of PDE4. Importantly, exogenous expression of DISC1 that binds to PDE4, but not mutant Htt, normalizes PDE4 activity and ameliorates anxiety-like phenotypes in the R6/2 model. Together, we propose that cross-seeding of mutant Htt and DISC1 and resultant changes in PDE4 may underlie the pathology, in particular the mental manifestations, of HD.

Introduction

Huntington's disease (HD) is a hereditary brain disease characterized by both motor and non-motor manifestations. Identification of the causal gene for Huntington's disease (HD), *Huntingtin* (*Htt*), has facilitated our understanding of the molecular pathways that mediate disease pathology. For instance, it has been demonstrated that functional and structural changes in mutant Htt elicited by the aberrant expansion of polyglutamine (polyQ) lead to the impairment of axonal transport and loss of medium spiny neurons. These deficits have been associated with motor dysfunction in HD (1-6). HD is also characterized by non-motor dysfunctions, such as depression and anxiety (7). Nonetheless, the molecular mechanisms underlying such mental manifestations in HD have not been well studied.

One of the leading mediators for cellular signaling involving higher brain functions is cyclic 3'5' adenosine monophosphate (cAMP) (8-10). cAMP levels are decreased in the cerebrospinal fluid from HD patients and in the brains from the Hdh^{Q111} knock-in mouse model for HD (11, 12). cAMP is degraded by various phosphodiesterases of which members of the phosphodiesterase-4 (PDE4) family play a major role including underpinning compartmentalized cAMP signaling in cells (13). Active site-directed small molecule inhibitors specific for PDE4, such as rolipram, together with targeted gene knockout and genetic studies, have shown that PDE4 regulates a wide range of brain functions, in particular mental states such as depression and anxiety (14-18). The activity of PDE4 is physiologically regulated at various levels, including intracellular localization, protein interaction, and posttranslational modifications (13, 18). One of the critical direct interactors with PDE4 is the intracellular scaffold protein DISC1 (16, 19-21). Physiological roles for DISC1 in biological pathways in brain development and neuro-signaling have been intensively studied for the past decade in various animal models (22-24). Yet, the significance of the DISC1-PDE4 interaction in neuropathological conditions is

poorly understood. Identification of a DISC1-PDE4 complex in conjunction with dysregulation of cAMP in HD would suggest the possibility that Htt might be involved in the DISC1-PDE4 pathway, but this mechanistic link has not been examined to date. Furthermore, DISC1 was previously shown to form insoluble aggregates (25, 26), but the structural basis of DISC1 aggregation and its neuropathological effects have not been investigated. Here we address a novel molecular mechanism involving the disturbance of DISC1-PDE4 interactions and behavioral changes through aggregation of DISC1 in HD.

Results

Augmentation of PDE4 activity in the R6/2 mice representing polyQ pathology of HD. We set out to determine a role for PDE4 in HD by first investigating its activity in R6/2 mouse model that is known to represents polyQ pathology of HD. Intriguingly, we observed a profound augmentation of PDE4 activity in both the cerebral cortex and striatum at 8 weeks (**Figure 1A**), prior to robust manifestation of motor dysfunction and intranuclear inclusions of Htt (27). Elevated PDE4 activity was also observed at up to 12 weeks of age (**Figure 1A**). These results may provide an explanation why rolipram has beneficial effects in the R6/2 model (28, 29). Consistent with our novel discovery *in vivo*, when we evaluated a cell model that stably expresses an N-terminal 1-67 amino acid fragment (corresponding to exon 1) of Htt with expanded polyQ (Htt67Q150) (30), we noted that PDE4 activity was increased by more than 3-fold (**Supplemental Figure 1**).

Regulation of PDE4 activity by a Htt-DISC1-PDE4 ternary protein complex. DISC1 interacts with dynactin (p150glued), *nuclear receptor corepressor (*N-CoR), pericentriolar material-1 protein (PCM1), and Kalirin-7, all of which also reportedly interact with huntingtin-associated protein 1 (HAP1) and/or Htt (22-24). The frequency of common binding

partners of DISC1 and Htt implied that these two proteins may interact either directly or indirectly. A recent bioinformatic approach also resulted in a similar proposal (31). As DISC1 and PDE4 proteins interact physically and functionally (16, 19, 32), we hypothesized that DISC1-PDE4, PDE4-Htt, and Htt-DISC1 proteins might interact. To evaluate this hypothesis, we conducted co-immunoprecipitation with the homogenates of whole mouse brains and identified the DISC1-PDE4, PDE4-Htt, and Htt-DISC1 protein interactions. (**Figures 1B and Supplemental Figure 2**). The DISC1-Htt and DISC1-PDE4 binding was more significant in striatum and cerebral cortex than in cerebellum (**Supplemental Figure 3A**).

Next, we asked whether these three proteins might form a ternary complex. Indeed, sequential co-immunoprecipitation demonstrated the formation of such a ternary complex (**Figure 1C**). PDE4B interacts with DISC1 in a unique manner (19), and has been implicated, from genetic association studies, to be an important DISC1 partner (16, 33). The PDE4B gene encodes several distinct isoforms of which the major ones are the PDE4B1 and PDE4B3 long forms and the PDE4B2 short form (34). We thus evaluated the binding of DISC1 with each of these isoforms and found that they each bound to DISC1 and to Htt. (**Supplemental Figure 3, B and C**).

Specific effect of polyQ expansion on the protein binding of Htt with DISC1. Given that PDE4, Htt, and DISC1 form a ternary protein complex, then how does polyQ expansion in Htt affect these protein interactions? We examined how the polyQ expansion affected Htt-DISC1 protein interaction by using an N-terminal 1-513 amino acid fragment of Htt with 18 residues of polyQ, or pathologically expanded 82 residues of polyQ (designated Htt513Q18 and Htt513Q82, respectively). The Htt513 and DISC1 interaction was augmented more than 2-fold when polyQ was expanded (**Figure 1D**). The increased binding was also observed when a shorter N-terminal fragment with an equal polyQ expansion (Htt67Q82) was used together with DISC1 (**Figure 1E**).

However, the binding of DISC1 with Htt513 was greater than that with Htt67 (**Supplemental Figure 4A**). These results indicate that amino acids 1-67 of Htt are sufficient to interact with DISC1, but that additional amino acids between 68 and 513 further facilitate the interaction. The effect of expanded polyQ on Htt-DISC1 binding was not observed in the interaction between PDE4B and Htt513 **(Supplemental Figure 4B)**, implying that the polyQ expansion has unique pathophysiological effects on the Htt-DISC1 interaction.

Selective sequestration of DISC1 into SDS-insoluble Htt aggregates in the R6/2 mice and HD's brains. One of the hallmarks of HD is the formation of SDS-resistant aggregates/inclusions of mutant Htt with expanded polyQ (35). DISC1 is also reportedly prone to aggregation (25, 26), but its pathophysiological significance is, as yet, unclear. Thus, we tested whether a pool of DISC1 could be detected in the SDS-resistant fraction of the brains from the R6/2 model, as well as HD patients, by using a filter trap assay. Significant increases in the levels of DISC1 in the SDS-resistant fractions from the cerebral cortex and striatum of R6/2 mice were observed, compared with those of normal mice (**Figure 2A**). Similar results were observed in the SDS-insoluble fractions from HD patients compared with those from normal controls (**Figure 2B**). In contrast, we did not find PDE4B immunoreactivity in the SDS-resistant fractions of any brain samples. Furthermore, by western blotting, we observed immunoreactivity of DISC1, but not that of PDE4B, on the top of the gel when we applied brain homogenates from R6/2 mice (**Supplemental Figure 5A**), further supporting the notion that a pool of DISC1 is insoluble to SDS in the R6/2 brain.

To test whether this insoluble DISC1 is associated with mutant Htt aggregation, we examined immunofluorescent tissue staining. We found that high-intensity DISC1 staining was co-localized with intranuclear aggregates of mutant Htt in both the cerebral cortex and striatum of R6/2 mice (**Figure 2C**). Furthermore, co-localization of DISC1 in the Htt aggregates was also

observed in the sections from the cortex and striatum of HD patients (**Figure 2D**). In contrast, no co-localization of PDE4B in Htt aggregates was detected in R6/2 mouse brains (**Supplemental Figure 5B**).

Cross-seeding between intrinsically amyloidogenic DISC1 and polyQ-expanded mutant Htt. The above results suggested that pathologically enhanced interaction of DISC1 and mutant Htt may selectively facilitate the sequestration of DISC1into the Htt aggregates. Therefore, we set out to evaluate possible biophysical mechanisms underlying the selective aggregation of DISC1 in HD. First, we aimed to reveal structural and physical properties of full-length DISC1 aggregates, which have not yet been fully characterized even though DISC1 has been shown to be aggregation-prone in nature (25, 26). We performed multiple biophysical assays *in vitro* and found that DISC1 formed amyloid fibers and that DISC1 aggregates reacted to an amyloid-specific dye, thioflavin T, at a level comparable to the typical amyloid, Htt67Q42 (35) (**Figure 3A**). The fibrillar morphology was confirmed by electron microscopy (**Figure 3B**). Furthermore, circular dichroism spectra of DISC1 aggregates showed a negative peak at 228 nm, indicating amyloid-like β-sheet-rich structures (36) (**Supplemental Figure 6**). These data show that DISC1 can form amyloid-like aggregates *in vitro*. As DISC1 does not contain glutamine/asparagine-rich domains that could induce aggregation, we examined a core region of DISC1 aggregates by mass spectrometry. Limited proteolysis of DISC1 aggregates with proteinase K treatment followed by MALDI-TOF mass analysis showed a single major peak at 2012.9 (m/Z) in the mass spectrum, which identified the core of DISC1 aggregates as the region consisting of residues 209-227 (**Figure 3C**).

We then examined the effects of Htt aggregates on the kinetics of DISC1 aggregation. As expected from the amyloidogenicity, DISC1 spontaneously formed aggregates, but the aggregation was not evident for the initial 2 h under the conditions tested. This 2 h lag time was

almost completely abolished by the addition of seeds (10% mol/mol) of DISC1 aggregates at the initiation of the reaction, indicating that DISC1 aggregates are self-propagating, a key feature of amyloidogenicity (37-39) (**Figure 3D**). More importantly, DISC1 aggregation was significantly accelerated with the addition of seeds of Htt67Q42 aggregates, but not with the addition of BSA aggregates, which were employed as a control (**Figure 3D**). These data reveal cross-seeding between DISC1 and mutant Htt, which is consistent with the marked co-localization of the two proteins in HD brains *in vivo* (**Figure 2D**).

The DISC1 aggregates that formed with seeds of Htt67Q42 aggregates showed an increase in the peak at 1620 cm^{-1} in Fourier-transform infrared (FT-IR) spectra, indicating a greater level of intermolecular β-sheet structures, compared to the DISC1 aggregates that were spontaneously formed in the absence of seeds (**Figure 3E**). Consistently, we found that the DISC1 aggregates formed with seeds of Htt67Q42 aggregates showed higher resistance to 2% SDS than did spontaneously formed DISC1 aggregates (**Figure 3F**). The altered structural and physical properties of the DISC1 aggregates also supported the cross-seeding between DISC1 and mutant Htt.

Reduced DISC1-PDE4 interactions by decreased soluble DISC1 levels in the R6/2 Mice. We then asked whether the physiological disposition of DISC1 might be impaired because of the selective sequestration of this protein into the Htt aggregates in HD pathology. First, we employed sedimentation analysis with homogenates of the cerebral cortex and striatum, and observed that the level of soluble DISC1, but not that of PDE4B, was reduced in R6/2 mice compared to that in wild-type mice (**Figure 4A**). DISC1 interacts with PDE4B in soluble fractions and regulates the enzymatic activity of PDE4 (16, 32). Thus, reduction in the levels of soluble DISC1 may result in a decrease in physiological DISC1-PDE4 interaction. In mouse brain homogenates, we showed a significant reduction of DISC1-PDE4 interaction in R6/2

compared with that in wild-type mice (**Figure 4B**). Furthermore, we addressed whether the reduction of DISC1-PDE4B interaction was elicited directly by the presence of mutant Htt. We added lysates of cells overexpressing Htt513Q18 or Htt513Q82 to cell lysates in which DISC1 and PDE4B interact, and examined how exogenous Htt513 proteins impact the DISC1-PDE4B binding. The addition of Htt513Q82 resulted in a significant reduction of pre-existing DISC1-PDE4B interactions, whereas that of Htt513Q18 did not (**Figure 4C**). Notably, as described above, augmented binding of Htt to DISC1 was observed with Htt513Q82 compared with Htt513Q18 (**Figure 1D**). Thus, a relative loss of DISC1's interaction with PDE4 is likely a major effect of the DISC1 sequestration into Htt aggregates due to the preferred binding of DISC1 with polyQ-expanded mutant Htt.

Htt-DISC1-PDE4 interactions for aberrant enhanced PDE4 activity in R6/2 mice.

We propose that sequestration of DISC1 into HD aggregates may disturb the regulatory effects of DISC1 on PDE4, resulting in aberrant augmentation of PDE4 enzymatic activity, which contributes to HD pathology. If this scenario is correct, supplementing wild-type DISC1 might ameliorate such increase of PDE4 activity in the models we have studied here. As described above, the overexpression of Htt67Q150 in neuro2a cells, in which substantial levels of endogenous DISC1 were expressed, (40) augmented PDE4 activity by 3- to 4-fold (**Supplemental Figure 1**). When we exogenously overexpressed wild-type DISC1 in the neuro2a cells carrying Htt67Q150, the aberrant augmentation of PDE4 activity was significantly ameliorated (**Supplemental Figure 7A**). Although these results are promising in terms of protecting cells against pathological PDE4 activation, we were curious why the beneficial effects of exogenous DISC1 were only partial. This may be because exogenously expressed DISC1 was also, at least in part, sequestered into Htt aggregates and could not fully regulate endogenous PDE4 activity.

We then set out to identify the region of DISC1 responsible for Htt binding, using a peptide array approach that has been used to successfully map the binding domain of DISC1 with protein interactors and PDE4 with various partner proteins (18, 19). We anticipated that a mutant DISC1 lacking a minimal domain for Htt interaction but maintaining PDE4 binding would not be sequestered into the Htt aggregates and thus would fully regulate PDE4 activity. Analyses of mouse and human DISC1 led to consistent results conserved between the two species, in which amino acids 206 to 220 of both of mouse and human DISC1 were crucial for binding with Htt (**Figure 5A**). Furthermore, in agreement with these observations from peptide arrays, mutant mouse DISC1 lacking amino acids 201-228 (Δ201-228-DISC1) displayed a dramatic reduction in DISC1-Htt513 binding in cells, compared with that in wild-type DISC1 (**Supplemental Figure 7B**). Importantly, this deletion showed minimal effects on DISC1-PDE4B1 and DISC1-PDE4B2 binding (**Supplemental Figure 7B**). Therefore, we expressed Δ201-228-DISC1 in neuro2a cells carrying the mutant Htt fragment. We then observed a greater extent of blockade, or complete normalization, against aberrantly augmented PDE4 activity, compared to the effects of wild-type DISC1 (**Supplemental Figure 7A**).

If aggregation of DISC1 is mediating the reduced PDE4 activity in HD brain, then the ectopic introduction of additional DISC1 should rescue the aberrant PDE4 activity seen in HD. Since our observations indicated that PDE4 activity was augmented in the striatum of 8-week-old R6/2 mice (**Figure 1A**), we next introduced exogenous DISC1 into the striatum of the 2-week-old mice by stereotaxic injection of a lentiviral vector of DISC1 connected with a green fluorescent protein Venus via IRES (DISC1/Venus). We then collected the DISC1/Venus-expressing cells from the striatum of the mice at 8 weeks by flow cytometry and measured PDE4 activity. Expression of wild-type DISC1 significantly decreased the aberrant PDE4 activity in R6/2 mice (**Figure 5B**). Introduction of DISC1Δ201-228 led to an even greater

effect, which is consistent with the observations from the cell model (**Figure 5B**). These results support the notion that pathological augmentation of PDE4 activity in HD pathology may be predominantly mediated by the partial loss of DISC1 that regulates PDE4 activity. This process is determined by the sequestration of DISC1 from the Htt-DISC1-PDE4 ternary complex as a result of specifically preferred binding and co-aggregation between mutant Htt and DISC1.

Significance of Htt-DISC1-PDE4 interactions on non-motor functions in R6/2 mice. Next, we examined the *in vivo* consequences of the disturbed DISC1-PDE4 interaction. We generated adeno-associated virus (AAV) encoding an N-terminal 1-316 amino acid fragment of mouse DISC1 which includes most of the binding sites for PDE4 but lacks the binding region for Htt (Δ201-228-nDISC1) (**Supplemental Figure 8**). We stereotaxically injected AAV encoding control EGFP or Δ201-228-nDISC1 that could interact with PDE4B isoforms but not Htt, into the striatum of 3-week-old R6/2 mice. We confirmed impairment of motor functions in R6/2, evident by deficits in rotarod performance and total distance in the open filed test (**Figures 5C and Supplemental Figure 9**). These behaviors were not affected by exogenous expression of Δ201-228-nDISC1 (**Figures 5C and Supplemental Figure 9**). By contrast, R6/2 mice showed a trend of spending less time in the center region of the open field test (**Figure 5D**). Although the difference was not statistically significant between R6/2 and wild-type mice, we took this change as an indication of anxiety-like manifestation (41, 42). Interestingly, the exogenous expression of Δ201-228-nDISC1, but not expression of a control protein EGFP, significantly altered the reduction of the center time and ameliorated the pathological behavior (**Figure 5D**). These results suggest the involvement of the DISC1-PDE4-Htt pathway specifically in the anxiety phenotype displayed by R6/2 mice.

Discussion

Here we demonstrate that the sequestration of intrinsically amyloidogenic DISC1, but not PDE4, into mutant Htt aggregates disturbed the proper formation of a Htt-DISC1-PDE4 ternary protein complex. This generates a PDE4 fraction out of physiological control by DISC1, thereby aberrantly increasing PDE4 activity (**Supplemental Figure 10**). Furthermore, our exploratory study *in vivo* suggests that this molecular pathway may underlie anxiety-like manifestations in the R6/2 model. The proposed molecular mechanism may account for the effects of rolipram, a specific PDE4 inhibitor, which ameliorate the pathological phenotype in these animals (28, 29). Finally, we hypothesize that this mechanism provides a novel molecular basis for the pathology and potentially the psychiatric symptoms, underpinning the reduced cAMP levels observed in both HD patients and model mice (11, 12).

We show here that the aggregation of DISC1 is significantly accelerated by the presence of mutant Htt aggregate seeds. Importantly, our structural analysis of DISC1 amyloid provided mechanistic insights into the efficient cross-seeding between mutant Htt and DISC1: the core region (residues 209-227) of DISC1 aggregates included the binding site for Htt (residues 206-220). This overlap might increase the chance of interactions between aggregation-prone core regions in distinct DISC1 molecules and thereby facilitate the sequestration of DISC1 into mutant Htt aggregates. In addition, the increase in amyloidogenicity of DISC1 aggregates by cross-seeding with mutant Htt may enhance the resistance to degradation and promote further recruitment of soluble DISC1 into mutant Htt aggregates.

The present report in cell biology and biophysics now provides at least two questions to be addressed in future studies. First, it will be important to clarify whether the sequestration of DISC1 into misfolded protein fractions and aggregates is specific to HD or more generally applied to other polyQ diseases. The present data from the R6/2 model that represents the polyQ pathology implies that DISC1 may also be involved in other polyQ diseases. Second, the next

study may use a full-length Htt mouse model to address the influence of Htt on broader aspects of HD pathology.

Recent studies have indicated that brain samples from a subgroup of patients with schizophrenia, bipolar disorder, or depression contain insoluble DISC1 and dysbindin, another protein that might be involved in the biology of mental functions (25, 43). Taken together, we provocatively propose that a selective network of misfolded proteins that are prone to be insoluble may underlie many aspects of brain dysfunctions, including psychiatric manifestations.

Methods

Plasmids and antibodies. The cDNA of full-length mouse DISC1 was subcloned into a pRK5 vector with an HA or myc tag at the N-terminus or with a pcDNA4 vector (Invitrogen) with a mys/His6 tag at the C-terminus. The cDNA of full-length human PDE4B1, 4B2, or 4B3 was subcloned into a pRK5 vector with an N-terminal HA tag. The cDNA of Htt67 or Htt513 containing 18 or 82 glutamine repeats was inserted into pCSII-CMV vector that includes EGFP at the C-terminus. For production of lentivirus, the cDNA of full-length or mutant mouse DISC1 with a C-terminal HA tag was subcloned into a pCSII-CMV-IRES-Venus plasmid. pCSII-CMV, pCAG-HIVgp, and pCAG-VSV-G plasmids were provided by the RIKEN BioResource Center. For production of AAV, the cDNA of full-length or mutant mouse DISC1was subcloned into a pAAV2 vector. For bacterial expression of DISC1 and Htt67Q42, the cDNA of human DISC1, Htt513Q18 and Htt67Q42 was inserted into a pCold-TF (Takara), pMAL (NEB) and pGEX6P2 (GE) vector including a His-tag at the C, N and N terminus, respectively. Rabbit polyclonal mouse DISC1 (m317C) and human DISC1 (h316C) antibodies were raised against the purified proteins of residues 317-852 in mouse DISC1 and residues 316-854 in human DISC1, respectively, in the Research Resources Center in RIKEN Brain Science Institute (**Supplemental**

Figure 2). A mouse monoclonal antibody for mouse DISC1 (M49) was produced with the purified protein of residues 317-852 as an antigen (MBL) (**Supplemental Figure 2**). The following commercial or published antibodies were also used: mouse monoclonal (Nacalai tesque) and rabbit polyclonal (MBL) antibodies for HA, myc and GFP tags, for mouse DISC1 (mEx3) (44), (D27) (45) and (2B3) (46), for human DISC1 (hEx2) (47) and for Htt (EM48 and MAB2144, Millipore), a sheep polyclonal anti-pan PDE4B antibody (34) and a mouse monoclonal antibody for β-actin (Abcam). Mouse, rabbit or sheep IgG (Santa Cruz) was also used as a control in co-immunoprecipitation experiments.

The R6/2 mice and autopsied brains from HD patients. Heterozygous Htt67 (corresponding to Htt exon 1) transgenic mice of R6/2 were obtained from Jackson Laboratory (Bar Harbor, ME) and maintained by ovarian transplantation of female R6/2 mice carrying about 130 CAG repeats. R6/2 transgenic and age-matched wild-type mice were anesthesized and the brains were removed, followed by separation of cerebral cortex and striatum. For measurement of PDE4 activity, storage of brains at -80 ^{o}C was minimized.

Measurement of PDE4 activity. PDE4 activity was assayed by our reported protocol (48). Briefly, brains or cells were homogenized in KHEM buffer (50 mM KCl, 10 mM EGTA, 1.92 mM $MgCl_2$, 1 mM DTT, and 50 mM HEPES, pH 7.2) containing protease inhibitor cocktail (Roche Applied Sciences), centrifuged, and the supernatant fraction was used to measure the PDE4 activity. Total cAMP specific phosphodiesterase activity was measured with 1 μM/l cAMP substrate concentration by using a fluorescence polarization assay (Molecular Devices) under linear conditions with and without the PDE4 inhibitor, rolipram at a concentration known to fully and selectively inhibit PDE4 (10 μM) (49).

Western blotting. A standard protocol was used, including 5-20% gradient acrylamide gels (ATTO). For detection, appropriate peroxidase-conjugated secondary antibodies (GE

Healthcare) were used in conjunction with a Supersignal West pico or femto chemiluminescent substrate (Thermo Fisher) to obtain images with LAS3000 (GE Healthcare).

Immunoprecipitation. Typically, cells or brains were lysed with RIPA buffer [50 mM Tris, pH 7.4, 150 mM NaCl, 1% NP40, 0.5% sodium deoxycholate, 0.1% SDS, and a protease inhibitor cocktail (Roche)]. Lysates were sonicated, cell debris was cleared by centrifugation at 200 g for 3 min at 4 ^{o}C, and the soluble fraction was subjected to immunoprecipitation with a primary antibody or an appropriate IgG control with Dynabeads protein G (Invitrogen). Green fluorescent protein (GFP) or monomeric red fluorescent protein (mRFP) was used as a negative control of binding partner. For sequential immunoprecipitation studies, Crosslink Magnetic IP/Co-IP Kit (Pierce) was used according to the manufacturer's protocol. The first and second immunoprecipitations were conducted with anti-DISC1 (m317C) and Htt (MAB2166) antibodies, respectively. An appropriate IgG was used as negative control for each reaction. For competitive binding experiments, lysates of the HEK293T cells overexpressing Htt513Q18-GFP or Htt513Q82-GFP were added to lysates of the HEK293T cells overexpressing DISC1-myc and PDE4B1-HA. The mixture was processed for immunoprecipitation with an anti-c-myc antibody.

Sedimentation assay. Samples (0.1 g) of cerebral cortex or striatum in wild-type or R6/2 mice were homogenized with 1 mL of RIPA buffer [50 mM Tris, pH 7.4, 150 mM NaCl, 1% NP40, 0.5% sodium deoxycholate, 0.1% SDS, and protease inhibitor cocktail (Roche)] by a digital homogenizer at 1,500 rpm for 15 strokes and sonicated for 10 sec (Branson sonifier, 15%). The homogenates were partially cleared by centrifugation at 200 g for 3 min at 4 ^{o}C and the supernatant (total fraction) was further centrifuged at 16,000 g for 15 min at 4 ^{o}C. Protein concentration of the total and supernatant fractions was determined by a BCA assay kit (Thermo Fisher) and 60 μg of protein/well of the total and supernatant fractions were used for immunoblotting.

Filter trap assay. Samples (0.1 g) of cerebral cortex or striatum in wild-type and R6/2 mice, or human controls and HD patients were homogenized with 1 mL of PBS including a protease inhibitor cocktail (Roche) by a digital homogenizer at 1,500 rpm for 15 strokes and sonicated for 10 sec (Branson sonifier, 15%). The homogenates were cleared by centrifugation at 200 g for 3 min at 4 ^{o}C and protein concentration of the supernatant (total fraction) was determined by a BCA assay kit (Thermo Fisher). 50 μg of protein/hole of the total brain homogenate was loaded onto a cellulose acetate membrane (0.2 μm, Advantec) in the dot blot apparatus (Bio-Rad) and the membrane was washed with 2% SDS, followed by immunoblotting. Loading of the same protein amounts on the membrane was confirmed by western blotting of the total fractions.

Immunohistochemistry. Mouse brains were fixed with 4% buffered paraformaldehyde, mounted with tissue mount (Shirai Kogyo), and frozen by carbon dioxide. The frozen brains were sectioned with a cryostat at 10 μm (Leica CM3050 S). Paraffin-embedded human brains were sectioned at 5 μm, followed by autoclaving in 10 mM citrate buffer, pH 6.0 at 121 ^{o}C for 3 min. Immunostaining was performed with a primary antibody (1:100-500), followed by Alexa Fluor 488- or 546-conjugated secondary antibodies (1:300) (Invitrogen). Vectorshield mountaing medium with DAPI (Vector Labs) was used to stain the nucleus. Fluorescent images of the serial-cut frozen or paraffin sections were acquired with a confocal microscope FV-1000D (Olympus) or C2 (Nikon).

Preparation of recombinant proteins and amyloid. Expression and purification of HisGST-tagged Htt67Q42 were reported previously(36). DISC1 protein was expressed at 15 ^{o}C in *E. coli.* [BL21 (DE3) Rosetta] as a fusion protein with a Hisx7-tag and trigger factor (TF) from a pCold TF (Takara) vector and was purified with 50 mM Tris-HCl buffer, pH 8.0, with 1 M NaCl and 2 mM β-mercaptoethanol under the native condition with Nickel agarose resin (GE

Healthcare). DISC1 protein was eluted with the same buffer containing 250 mM imidazole, concentrated, and passed through a 1000K filter (Millipore) to remove preexisting aggregates. Staining with Coomassie Brilliant Blue showed that DISC1 was >90% pure and the protein concentration was determined at an extinction coefficient of HisTF-DISC1 (85,600 $mM^{-1}cm^{-1}$). For amyloid formation, typically 1 mL of 5 μM protein solution with 10 units of turbo3C protease (Accelagen) to cleave the tag was rotated in an end-over-end manner in a 2-mL tube at 37 ^{o}C (36).

Characterization of DISC1 amyloid in vitro. The presence of amyloid-like structures in DISC1 aggregates was examined by an amyloid-specific fluorescent dye, thioflavine T (Sigma). The fluorescence of thioflavine T (excitation, 442 nm; emission, 483 nm) in 50 mM Na-glycine buffer (pH 8.0) including 12.5 μM thioflavine T and 5 μM DISC1 aggregates was measured with a fluorescence plate reader (ARVO MX, PerkinElmer) (36). For morphological observation of DISC1 aggregates with transmission electron microscopy (JEM 1200EX, JEOL), an aliquot of 2 μM DISC1 aggregates was adsorbed onto carbon-coated 400-mesh copper grids, followed by 2% paraformaldehyde and 2% glutaraldehyde in 100 mM sodium phosphate buffer. The samples were negatively stained with 2% sodium phosphotungstic acid. Far-UV CD and FT-IR spectra of DISC1 aggregates were measured as described previously (36, 50). A core region in DISC1 aggregates was identified with a 4800 plus MALDI-TOF/TOF Analyzer (AB SCIEX) as previously reported (51). The kinetics of DISC1 aggregation was monitored by the absorbance (turbidity) at 405 nm, with 10 mM DISC1 protein in 5 mM potassium phosphate buffer containing 150 mM sodium chloride (pH 7.4), and 2 units of turbo3C protease in the absence or presence of seeds of indicated aggregates [10% (mol/mol)] with a plate reader in a 96-well format (SpectraMax M2, Molecular Devices). The aggregate seeds were prepared by sonication (Branson sonifier, 15%) of 5 mM protein aggregates for 10 sec. The plate reader instrument

agitates a 96-well plate for 5 sec every 2 min. A filter trap assay was performed with 10 mg of Htt67Q42, DISC1 or BSA aggregates by using a cellulose acetate membrane (0.2 mm, Advantec) in the dot blot apparatus (Bio-Rad). After the protein was loaded, the membrane was washed with 5 mM potassium phosphate buffer (pH 7.4) with 2% SDS, followed by detection of signals with Sypro Ruby staining (Bio-Rad).

Peptide array. MBP-Htt513Q18 protein was expressed at 20^{o}C in *E. coli.* BL21 (DE3) Rosetta as a fusion protein with an N-terminal Hisx7-tag and purified as TF-DISC1. Coomassie Brilliant Blue staining showed that MBP-Htt513Q18 was >90% pure, and the protein concentration was determined by an extinction coefficient of MBP-Htt513Q18 (37,940 $mM^{-1}cm^{-1}$). Peptide arrays of mouse and human DISC1 were generated as previously reported (19, 52, 53). 1 μg of MBP alone or MBP-Htt513Q18 protein in PBS was overlaid to the peptide array. The array was washed with PBS, followed by detection as previously reported (19, 53).

Production of lentivirus and injection into mice. HEK293T cells were transfected with a pCSII-CMV-mouse DISC1- or Δ201−228−DISC1-IRES-Venus plasmid together with pCAG-HIVgp and pCAG-VSV-G plasmids, and forskolin (Sigma) was added to the culture medium (10 μM). Purification of lentivirus was performed as previously reported (53), with the exception that the lentivirus was concentrated with Lenti-X Concentrator (Clontech) and the pellet was resuspended with MACS Neurobasal media (Miltenyi Biotec) containing MACS B27 plus (Miltenyi Biotec), penicillin and streptomycin (Nacalai). Stereotaxic injections were bilaterally placed at 0 and 1.0 mm anterior to the bregma, 2.0 mm lateral to the sagittal suture, and 2.0 mm below the skull surface in 2 week-old wild-type or R6/2 mice. 1 μL of lentivirus (200 μL of lentivirus purified from 10 mL culture) was injected with the rate of 0.1 μL/min by a microinjector (Narishige). Immunohistochemical analyses with frozen sections of the mice confirmed the expression of Venus and DISC1 in striatum. At 8 weeks, the striatum of the mice

was removed, minced on ice and treated with a Papain Dissection System (Worthington) to separate cells. The cells were treated with propidium idodide (Nacalai), and the Venus-expressing and propidium iodide-negative cells were collected by flow cytometry (FACSAria, BD), followed by centrifugation at 1,000 g for 15 min at 4 ^{o}C.

Behavioral analysis of mice. Following injection of AAV in striatum, the behavioral tests were performed for wild-type and R6/2 mice at the age of 8-10 weeks. The open filed test was performed as previously described (54). Briefly, each mouse was placed in the center of the open field [50×50×40 (H) cm] and allowed to move freely for 15 min. Distance traveled (cm) and time spent (%) in the center area (30%) of the field or in the four corner squares of the 5×5 subdivisions were measured every 1 min and analyzed by TimeOFCR4 (O'Hara & Co.). For the rotarod performance test, a mouse was placed on a rotating rod (Muromachi Kikai) and the latency time the mouse was able to run on the rod was measured. The speed of rotation on day 1 was 4 rpm and was increased from 4 to 40 rpm over a 4-min period and then kept at 40 rpm for another 1 min from days 2 to 5. Mice were tested in one trial for 2 min on day 1 and in four trials with a maximum time of 300 sec (intervals between trials were 20–30 sec) on days 2 to 5. The latency time of mice on the rotating rod was recorded by the instrument.

Statistical analysis. For analyses of two groups, *P*-values were determined by *t*-test. For analyses of three or more groups, *P*-values were determined by one-way ANOVA followed by Bonferroni post hoc corrections. The *P* values of <0.05 (*), <0.01 (**), and <0.001 (***) were considered to be statistically significant.

Study approval. All of the animal experiments were performed in compliance with relevant laws and guidelines issued by RIKEN and JHU. Samples of autopsied brains were obtained from the Harvard Brain Tissue Resource Center at McLean Hospital in Belmont, Massachusetts.

Author contributions

M.T., K.I. and A.S. designed the experiments. M.T., K.I., Y.N., R.E., N.T., Y.K., M.K. S.K. and N.N. performed the cell biology, mouse and structural biology experiments. S.H. and E.T. measured PDE4 activity. A.G., E.H. and M.H. performed peptide array experiments. M.T., K.I., M.H. and A.S. wrote the paper.

Acknowledgments

We thank Drs. Pamela Talalay and Mari Kondo for critical reading of this manuscript, Y. Lema for organizing the figures and manuscript, Mao Yamaguchi and Mizue Honda for help with genotyping of mice and ovarian transplantation, Yumiko Ohhashi for advice on structural analyses of protein aggregates, and Naomi Takahashi for help with subcloning. DNA sequencing, mass spectrometry, flow cytometry and electron microscopic analyses were performed at RIKEN Brain Science Institute Research Resources Center. This work was supported by USPHS grants MH-084018 (A.S.), MH-094268 Silvio O. Conte center (A.S.), MH-069853 (A.S.), MH-085226 (A.S.), MH-088753 (A.S.), MH-092443 (A.S.), MH-105660 (A.S. and K.I.) and MH-96208 (K.I.), grants from Stanley (A.S.), RUSK (A.S.), S-R foundations (A.S.), NARSAD (A.S. and K.I.), and Maryland Stem Cell Research Fund (A.S. and K.I.), the Next program LS129 (M.T.), Grant-in-Aid for Young Scientists (A) 22680030 (M.T.), Young Scientists (B) 23700398 (R.E.), Encouragement of Scientists (Y.N.) from MEXT, Japan and Japan Intractable Diseases Research Foundation (M.T.). Medical Research Council (M.D.H.), Scottish Enterprise (M.D.H.).

References

1. Crook ZR, Housman D. Huntington's disease: can mice lead the way to treatment? *Neuron.* 2011;69(3):423-435.
2. Di Prospero NA, Fischbeck KH. Therapeutics development for triplet repeat expansion diseases. *Nat Rev Genet.* 2005;6(10):756-765.
3. Saudou F, Humbert S. The biology of Huntington's disease. *Handb Clin Neurol.* 2008;89(619-629.
4. Labbadia J, Morimoto RI. Huntington's disease: underlying molecular mechanisms and emerging concepts. *Trends Biochem Sci.* 2013.
5. Orr HT, Zoghbi HY. Trinucleotide repeat disorders. *Annu Rev Neurosci.* 2007;30(575-621.
6. An MC, Zhang N, Scott G, Montoro D, Wittkop T, Mooney S, Melov S, Ellerby LM. Genetic correction of Huntington's disease phenotypes in induced pluripotent stem cells. *Cell Stem Cell.* 2012;11(2):253-263.
7. Craufurd D, Snowden J. In: Gillian Bates PH, Lesley Jones ed. *Huntington's Disease*. OXFORD UNIVERSITY PRESS; 2002:62-94.
8. Kandel ER. The molecular biology of memory: cAMP, PKA, CRE, CREB-1, CREB-2, and CPEB. *Mol Brain.* 2012;5(14.
9. Duman RS. Synaptic plasticity and mood disorders. *Mol Psychiatry.* 2002;7 Suppl 1(S29-34.
10. Arnsten AF, Wang MJ, Paspalas CD. Neuromodulation of thought: flexibilities and vulnerabilities in prefrontal cortical network synapses. *Neuron.* 2012;76(1):223-239.
11. Gines S, Seong IS, Fossale E, Ivanova E, Trettel F, Gusella JF, Wheeler VC, Persichetti F, MacDonald ME. Specific progressive cAMP reduction implicates energy deficit in

presymptomatic Huntington's disease knock-in mice. *Hum Mol Genet.* 2003;12(5):497-508.

12. Cramer H, Warter JM, Renaud B. Analysis of neurotransmitter metabolites and adenosine 3',5'-monophosphate in the CSF of patients with extrapyramidal motor disorders. *Adv Neurol.* 1984;40(431-435.

13. Conti M, Beavo J. Biochemistry and physiology of cyclic nucleotide phosphodiesterases: essential components in cyclic nucleotide signaling. *Annu Rev Biochem.* 2007;76(481-511.

14. Menniti FS, Faraci WS, Schmidt CJ. Phosphodiesterases in the CNS: targets for drug development. *Nat Rev Drug Discov.* 2006;5(8):660-670.

15. O'Donnell JM, Zhang HT. Antidepressant effects of inhibitors of cAMP phosphodiesterase (PDE4). *Trends Pharmacol Sci.* 2004;25(3):158-163.

16. Millar JK, Pickard BS, Mackie S, James R, Christie S, Buchanan SR, Malloy MP, Chubb JE, Huston E, Baillie GS, et al. DISC1 and PDE4B are interacting genetic factors in schizophrenia that regulate cAMP signaling. *Science (New York, NY.* 2005;310(5751):1187-1191.

17. Burgin AB, Magnusson OT, Singh J, Witte P, Staker BL, Bjornsson JM, Thorsteinsdottir M, Hrafnsdottir S, Hagen T, Kiselyov AS, et al. Design of phosphodiesterase 4D (PDE4D) allosteric modulators for enhancing cognition with improved safety. *Nat Biotechnol.* 2010;28(1):63-70.

18. Houslay MD. Underpinning compartmentalised cAMP signalling through targeted cAMP breakdown. *Trends Biochem Sci.* 2010;35(2):91-100.

19. Murdoch H, Mackie S, Collins DM, Hill EV, Bolger GB, Klussmann E, Porteous DJ, Millar JK, Houslay MD. Isoform-selective susceptibility of DISC1/phosphodiesterase-4

complexes to dissociation by elevated intracellular cAMP levels. *J Neurosci.* 2007;27(35):9513-9524.

20. Kvajo M, McKellar H, Drew LJ, Lepagnol-Bestel AM, Xiao L, Levy RJ, Blazeski R, Arguello PA, Lacefield CO, Mason CA, et al. Altered axonal targeting and short-term plasticity in the hippocampus of Disc1 mutant mice. *Proc Natl Acad Sci U S A.* 2011;108(49):E1349-1358.

21. Harrison PJ, Weinberger DR. Schizophrenia genes, gene expression, and neuropathology: on the matter of their convergence. *Mol Psychiatry.* 2005;10(1):40-68; image 45.

22. Brandon NJ, Sawa A. Linking neurodevelopmental and synaptic theories of mental illness through DISC1. *Nat Rev Neurosci.* 2011;12(12):707-722.

23. Johnstone M, Thomson PA, Hall J, McIntosh AM, Lawrie SM, Porteous DJ. DISC1 in schizophrenia: genetic mouse models and human genomic imaging. *Schizophr Bull.* 2011;37(1):14-20.

24. Narayan S, Nakajima K, Sawa A. DISC1: a key lead in studying cortical development and associated brain disorders. *Neuroscientist.* 2013;19(5):451-464.

25. Leliveld SR, Bader V, Hendriks P, Prikulis I, Sajnani G, Requena JR, Korth C. Insolubility of disrupted-in-schizophrenia 1 disrupts oligomer-dependent interactions with nuclear distribution element 1 and is associated with sporadic mental disease. *J Neurosci.* 2008;28(15):3839-3845.

26. Atkin T, Kittler J. DISC1 and the aggresome: a disruption to cellular function? *Autophagy.* 2012;8(5):851-852.

27. Davies SW, Turmaine M, Cozens BA, DiFiglia M, Sharp AH, Ross CA, Scherzinger E, Wanker EE, Mangiarini L, Bates GP. Formation of neuronal intranuclear inclusions

underlies the neurological dysfunction in mice transgenic for the HD mutation. *Cell.* 1997;90(3):537-548.

28. DeMarch Z, Giampa C, Patassini S, Bernardi G, Fusco FR. Beneficial effects of rolipram in the R6/2 mouse model of Huntington's disease. *Neurobiol Dis.* 2008;30(3):375-387.

29. Giampa C, Middei S, Patassini S, Borreca A, Marullo F, Laurenti D, Bernardi G, Ammassari-Teule M, Fusco FR. Phosphodiesterase type IV inhibition prevents sequestration of CREB binding protein, protects striatal parvalbumin interneurons and rescues motor deficits in the R6/2 mouse model of Huntington's disease. *Eur J Neurosci.* 2009;29(5):902-910.

30. Wang GH, Mitsui K, Kotliarova S, Yamashita A, Nagao Y, Tokuhiro S, Iwatsubo T, Kanazawa I, Nukina N. Caspase activation during apoptotic cell death induced by expanded polyglutamine in N2a cells. *Neuroreport.* 1999;10(12):2435-2438.

31. Boxall R, Porteous DJ, Thomson PA. DISC1 and Huntington's disease--overlapping pathways of vulnerability to neurological disorder? *PLoS One.* 2011;6(1):e16263.

32. Carlyle BC, Mackie S, Christie S, Millar JK, Porteous DJ. Co-ordinated action of DISC1, PDE4B and GSK3beta in modulation of cAMP signalling. *Mol Psychiatry.* 2011;16(7):693-694.

33. Fatemi SH, King DP, Reutiman TJ, Folsom TD, Laurence JA, Lee S, Fan YT, Paciga SA, Conti M, Menniti FS. PDE4B polymorphisms and decreased PDE4B expression are associated with schizophrenia. *Schizophr Res.* 2008;101(1-3):36-49.

34. Huston E, Lumb S, Russell A, Catterall C, Ross AH, Steele MR, Bolger GB, Perry MJ, Owens RJ, Houslay MD. Molecular cloning and transient expression in COS7 cells of a novel human PDE4B cAMP-specific phosphodiesterase, HSPDE4B3. *Biochem J.* 1997;328 (Pt 2)(549-558.

35. Scherzinger E, Lurz R, Turmaine M, Mangiarini L, Hollenbach B, Hasenbank R, Bates GP, Davies SW, Lehrach H, Wanker EE. Huntingtin-encoded polyglutamine expansions form amyloid-like protein aggregates in vitro and in vivo. *Cell.* 1997;90(3):549-558.

36. Nekooki-Machida Y, Kurosawa M, Nukina N, Ito K, Oda T, Tanaka M. Distinct conformations of in vitro and in vivo amyloids of huntingtin-exon1 show different cytotoxicity. *Proc Natl Acad Sci U S A.* 2009;106(24):9679-9684.

37. Harper JD, Lansbury PT, Jr. Models of amyloid seeding in Alzheimer's disease and scrapie: mechanistic truths and physiological consequences of the time-dependent solubility of amyloid proteins. *Annu Rev Biochem.* 1997;66(385-407.

38. Eisenberg D, Jucker M. The amyloid state of proteins in human diseases. *Cell.* 2012;148(6):1188-1203.

39. Tessier PM, Lindquist S. Unraveling infectious structures, strain variants and species barriers for the yeast prion [PSI+]. *Nat Struct Mol Biol.* 2009;16(6):598-605.

40. Mao Y, Ge X, Frank CL, Madison JM, Koehler AN, Doud MK, Tassa C, Berry EM, Soda T, Singh KK, et al. Disrupted in schizophrenia 1 regulates neuronal progenitor proliferation via modulation of GSK3beta/beta-catenin signaling. *Cell.* 2009;136(6):1017-1031.

41. Menalled L, El-Khodor BF, Patry M, Suarez-Farinas M, Orenstein SJ, Zahasky B, Leahy C, Wheeler V, Yang XW, MacDonald M, et al. Systematic behavioral evaluation of Huntington's disease transgenic and knock-in mouse models. *Neurobiol Dis.* 2009;35(3):319-336.

42. Cowin RM, Bui N, Graham D, Green JR, Grueninger S, Yuva-Paylor LA, Syed AU, Weiss A, Paylor R. Onset and progression of behavioral and molecular phenotypes in a

novel congenic R6/2 line exhibiting intergenerational CAG repeat stability. *PLoS One.* 2011;6(12):e28409.

43. Ottis P, Bader V, Trossbach SV, Kretzschmar H, Michel M, Leliveld SR, Korth C. Convergence of two independent mental disease genes on the protein level: recruitment of dysbindin to cell-invasive disrupted-in-schizophrenia 1 aggresomes. *Biol Psychiatry.* 2011;70(7):604-610.

44. Ishizuka K, Chen J, Taya S, Li W, Millar JK, Xu Y, Clapcote SJ, Hookway C, Morita M, Kamiya A, et al. Evidence that many of the DISC1 isoforms in C57BL/6J mice are also expressed in 129S6/SvEv mice. *Mol Psychiatry.* 2007;12(10):897-899.

45. Schurov IL, Handford EJ, Brandon NJ, Whiting PJ. Expression of disrupted in schizophrenia 1 (DISC1) protein in the adult and developing mouse brain indicates its role in neurodevelopment. *Mol Psychiatry.* 2004;9(12):1100-1110.

46. Shahani N, Seshadri S, Jaaro-Peled H, Ishizuka K, Hirota-Tsuyada Y, Wang Q, Koga M, Sedlak TW, Korth C, Brandon NJ, et al. DISC1 regulates trafficking and processing of APP and Abeta generation. *Mol Psychiatry.* 2015;20(874-879.

47. Ishizuka K, Kamiya A, Oh EC, Kanki H, Seshadri S, Robinson JF, Murdoch H, Dunlop AJ, Kubo K, Furukori K, et al. DISC1-dependent switch from progenitor proliferation to migration in the developing cortex. *Nature.* 2011;473(7345):92-96.

48. Takimoto E, Champion HC, Li M, Belardi D, Ren S, Rodriguez ER, Bedja D, Gabrielson KL, Wang Y, Kass DA. Chronic inhibition of cyclic GMP phosphodiesterase 5A prevents and reverses cardiac hypertrophy. *Nat Med.* 2005;11(2):214-222.

49. Houslay MD, Adams DR. PDE4 cAMP phosphodiesterases: modular enzymes that orchestrate signalling cross-talk, desensitization and compartmentalization. *Biochem J.* 2003;370(Pt 1):1-18.

50. Ohhashi Y, Ito K, Toyama BH, Weissman JS, Tanaka M. Differences in prion strain conformations result from non-native interactions in a nucleus. *Nat Chem Biol.* 2010;6(3):225-230.

51. Suzuki G, Shimazu N, Tanaka M. A yeast prion, Mod5, promotes acquired drug resistance and cell survival under environmental stress. *Science (New York, NY.* 2012;336(6079):355-359.

52. Bolger GB, Baillie GS, Li X, Lynch MJ, Herzyk P, Mohamed A, Mitchell LH, McCahill A, Hundsrucker C, Klussmann E, et al. Scanning peptide array analyses identify overlapping binding sites for the signalling scaffold proteins, beta-arrestin and RACK1, in cAMP-specific phosphodiesterase PDE4D5. *Biochem J.* 2006;398(1):23-36.

53. Hayashi-Takagi A, Takaki M, Graziane N, Seshadri S, Murdoch H, Dunlop AJ, Makino Y, Seshadri AJ, Ishizuka K, Srivastava DP, et al. Disrupted-in-Schizophrenia 1 (DISC1) regulates spines of the glutamate synapse via Rac1. *Nat Neurosci.* 2010;13(3):327-332.

54. Takashima N, Odaka YS, Sakoori K, Akagi T, Hashikawa T, Morimura N, Yamada K, Aruga J. Impaired cognitive function and altered hippocampal synapse morphology in mice lacking Lrrtm1, a gene associated with schizophrenia. *PLoS One.* 2011;6(7):e22716.

Figure legends

Figure 1. PDE4 activity could be regulated by the newly identified Htt-DISC1-PDE4 ternary protein complex.

(A) PDE4 activities of the homogenates of cerebral cortex (left) and striatum (right) in R6/2 mice were increased compared with those in wild-type (WT) at 8 and 12 weeks of age. Error bars denote S.E.M. **P*<0.05, ***P*<0.01, ****P*<0.001.

(B) Protein complex of Htt-DISC1-PDE4B in cerebral cortex of wild-type mice. Brain homogenates were immunoprecipitated by an anti-DISC1 (mEx3), anti-PDE4B (pan PDE4B), or anti-Htt (MAB2144) antibody or IgG control, followed by immunoblotting with an anti-Htt (MAB2144), anti-DISC1 (D27) or anti-PDE4B (pan PDE4B) antibody.

(C) Formation of Htt-DISC1-PDE4B tertiary protein complex in cerebral cortex of wild-type mice was detected with sequential co-immunoprecipitation. Brain homogenates were immunoprecipitated by an anti-DISC1 (m317C) (1st IP) then the immunoprecipitates were immunoprecipitated by Htt antibody (MAB2166) (2nd IP), followed by immunoblotting with an anti-Htt (MAB2166), anti-DISC1 (2B3) or anti-PDE4B (pan PDE4B) antibody. Negative control was immunoprecipitated by IgG.

(D) Increased binding of Htt513 and DISC1 with expansion of polyQ in HEK293T cells by co-immunoprecipitation. Error bars denote S.E.M. **P*<0.05.

(E) Increased binding of Htt67 and DISC1 with expansion of polyQ in HEK293T cells by co-immunoprecipitation. Error bars denote S.E.M. ****P*<0.001.

Figure 2. DISC1, but not PDE4B, is sequestered into insoluble Htt aggregates in HD.

(A) Filter trap assay with homogenates of cerebral cortex or striatum from 12-week-old R6/2 mice showed significantly increased levels of Htt (EM48) (top) and DISC1 (mEx3) (middle), but

not PDE4B (pan PDE4B) (bottom) in the SDS-resistant fraction, compared with those from wild-type (WT) mice. Error bars denote S.E.M. *P<0.05, **P<0.01.

(B) Filter trap assay with homogenates of cerebral cortex or striatum showed significantly increased levels of Htt (EM48) (top) and DISC1 (h2p) (middle), but not PDE4B (pan PDE4B) (bottom) in the SDS-resistant fraction from HD patients (HD), compared to those from controls (Con). Error bars denote S.E.M. *P<0.05, ***P<0.001.

(C) Immunostaining of frozen sections of cerebral cortex (left) or striatum (right) demonstrated that DISC1 was colocalized with intranuclear inclusions of mutant Htt in 12-week-old R6/2 mice. Green, Htt (EM48); red, DISC1 (m317C); blue, DAPI (the nucleus). Arrowheads show intranuclear inclusions. Scale bar, 10 μm.

(D) Immunostaining of paraffin sections of cerebral cortex (left half) or striatum (right half) in HD patients (HD) and human controls (Con) was performed with anti-Htt (EM48) (green, left) and anti-DISC1 (h316C) (red) antibodies. Nucleus was stained by DAPI (blue). Merged images are shown on the right. Arrowheads show intranuclear inclusions. Scale bar, 10 μm.

Figure 3. Aggregation of intrinsically amyloidogenic DISC1 is accelerated by cross-seeding with polyQ-expanded mutant Htt.

(A) Thioflavin T (ThT) fluorescent intensities of DISC1 and Htt67Q42 aggregates were significantly higher than that of BSA aggregates. Error bars denote S.E.M. ***P<0.001.

(B) Fibrillar morphology of typical DISC1 amyloid shown by transmission electron microscopy. Scale bar, 100 nm.

(C) MALDI-TOF mass spectrum of DISC1 aggregates digested by proteinase K indentified a major mass peak at 2012.9 m/Z corresponding to residues 209-227 in DISC1 as the core of DISC1 aggregates.

(D) Aggregation of DISC1, which was monitored by the absorbance (turbidity) at 405 nm, was significantly accelerated by the Htt67Q42 aggregate seeds but not by BSA aggregates.

(E) FT-IR spectra revealed that the DISC1 aggregates formed in the presence of Htt67Q42 aggregate seeds (grey) contained more intermolecular β-sheet structures (arrowheads) than did spontaneously formed DISC1 aggregates (black).

(F) The DISC1 aggregates formed in the presence of Htt67Q42 aggregate seeds showed higher resistance to 2% SDS than spontaneously formed DISC1 aggregates in the filter trap assay with Sypro Ruby staining. Error bars denote S.E.M.

Figure 4. DISC1-PDE4 interactions are reduced by decreased soluble DISC1 levels in the R6/2 mice.

(A) Soluble DISC1, but not soluble PDE4B levels in supernatant fractions (Sup) were reduced in cerebral cortex (top) and striatum (bottom) from 12-week-old R6/2 mice, compared to those from wild-type (WT) mice. Total DISC1 and PDE4B levels in total homogenates (Total) were not changed between WT and R6/2 mice. β-actin is a loading control. DISC1 antibodies (mEx3 for cortex, m317C for striatum) were used for immunblotting. Error bars denote S.E.M. *P<0.05.

(B) Binding between PDE4B and DISC1 in 12-week-old R6/2 mouse brains was decreased compared to that of wild-type (WT) brains. Immunoprecitation was performed by an anti-pan PDE4B antibody, followed by immunoblotting with anti-DISC1 antibody (D27). Error bars denote S.E.M. **P<0.01.

(C) Exogenous addition of Htt513Q82, but not Htt513Q18, significantly reduced DISC1-PDE4B interactions in HEK293T cells. Lysates of the cells overexpressing GFP alone (−), Htt513Q18-GFP (Q18), or Htt513Q82-GFP (Q82) were added to lysates of the cells overexpressing DISC1-myc and PDE4B1-HA. Mixtures were processed for immunoprecipitation

with an anti-c-myc antibody, followed by immunoblotting. Error bars denote S.E.M. *P<0.05, **P<0.01.

Figure 5. Aberrantly enhanced PDE4 activity and anxiety levels in the R6/2 mice are recovered by exogenous DISC1 expression.

(**A**) The 25mer-peptides #40-#42 [residues 194-228 for mouse DISC1 (left), residues 196-230 for human DISC1 (right)] in DISC1 showed binding to maltose binding protein (MBP)-Htt513Q18 (bottom) but not MBP alone (top) on peptide array. A black line corresponds to the amyloid core region identified by limited proteolysis and mass spectrometry (see **Figure 3C**).

(B) Aberrant augmentation of PDE4 activity in striatum of R6/2 mice was normalized with Wt or Δ201-228-DISC1. Error bars denote S.E.M. *P<0.05, **P<0.01.

(C) The locomotor activity of R6/2 mice was not affected by expression of Δ201-228-nDISC1. Total distance moved in the open field test was measured in mice at 8 weeks. Error bars denote S.E.M. n=15, 15, 18, 17 for WT+EGFP, WT+Δ201-228-nDISC1, R6/2+EGFP, R6/2+Δ201-228-nDISC1 mice, respectively. **P<0.01, ***P<0.001.

(D) The anxiety levels in R6/2 mice were reduced by expression of Δ201-228-nDISC1. The time spent in a center region in the open field test was measured in mice at 8 weeks. Error bars denote S.E.M. n=15, 15, 18, 17 for WT+EGFP, WT+Δ201-228-nDISC1, R6/2+EGFP, R6/2+Δ201-228-nDISC1 mice, respectively. *P<0.05.

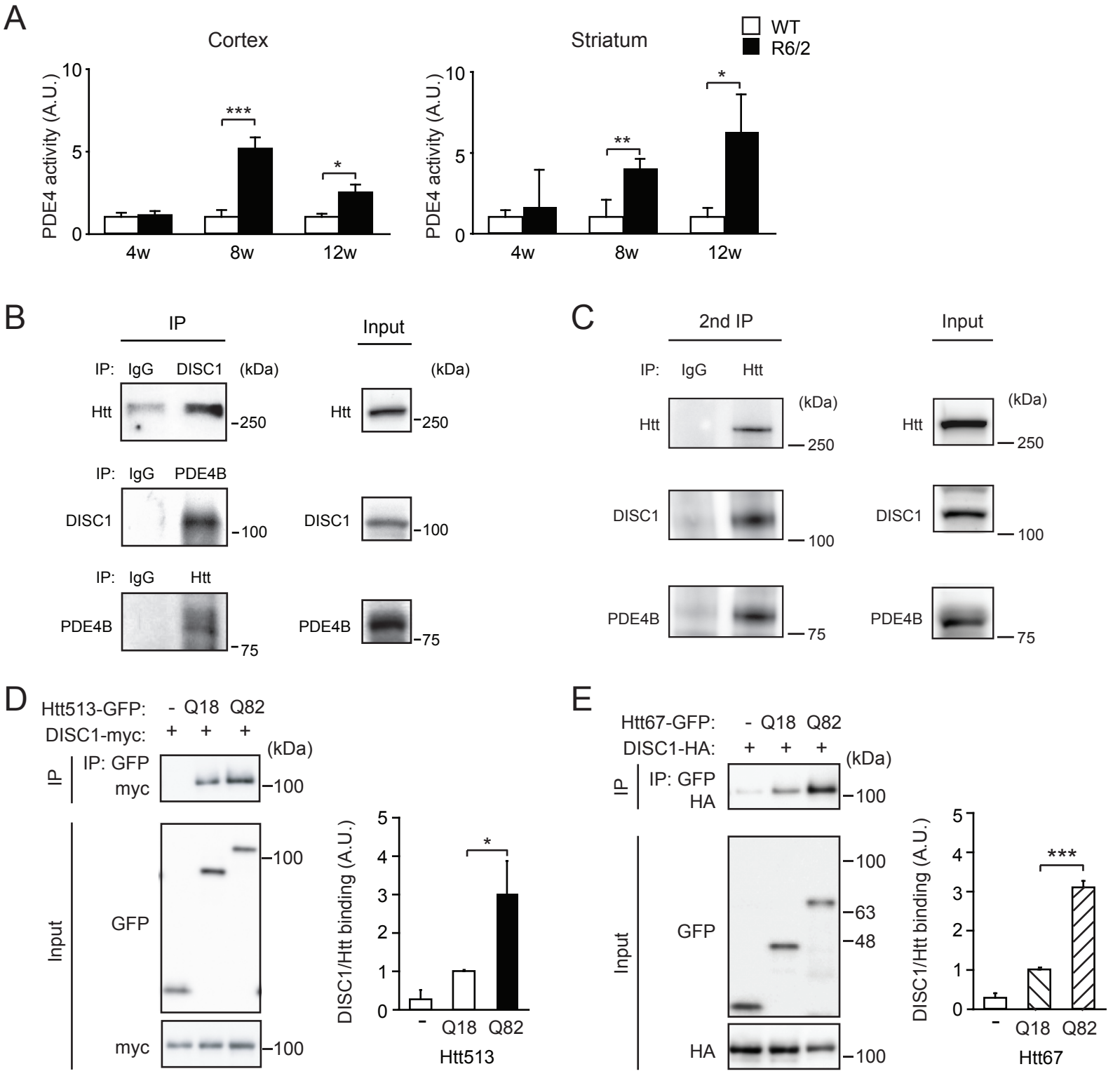

Figure 1. PDE4 activity could be regulated by the newly identified Htt-DISC1-PDE4 ternary protein complex.

(A) PDE4 activities of the homogenates of cerebral cortex (left) and striatum (right) in R6/2 mice were increased compared with those in wild-type (WT) at 8 and 12 weeks of age. Error bars denote S.E.M. **P*<0.05, ***P*<0.01, ****P*<0.001.

(B) Protein complex of Htt-DISC1-PDE4B in cerebral cortex of wild-type mice. Brain homogenates were immunoprecipitated by an anti-DISC1 (mEx3), anti-PDE4B (pan PDE4B), or anti-Htt (MAB2144) antibody or IgG control, followed by immunoblotting with an anti-Htt (MAB2144), anti-DISC1 (D27) or anti-PDE4B (pan PDE4B) antibody.

(C) Formation of Htt-DISC1-PDE4B tertiary protein complex in cerebral cortex of wild-type mice was detected with sequential co-immunoprecipitation. Brain homogenates were immunoprecipitated by an anti-DISC1 (m317C) (1st IP) then the immunoprecipitates were immunoprecipitated by Htt antibody (MAB2166) (2nd IP), followed by immunoblotting with an anti-Htt (MAB2166), anti-DISC1 (2B3) or anti-PDE4B (pan PDE4B) antibody. Negative control was immunoprecipitated by IgG.
(D) Increased binding of Htt513 and DISC1 with expansion of polyQ in HEK293T cells by co-immunoprecipitation. Error bars denote S.E.M. *P<0.05.
(E) Increased binding of Htt67 and DISC1 with expansion of polyQ in HEK293T cells by co-immunoprecipitation. Error bars denote S.E.M. ***P<0.001.

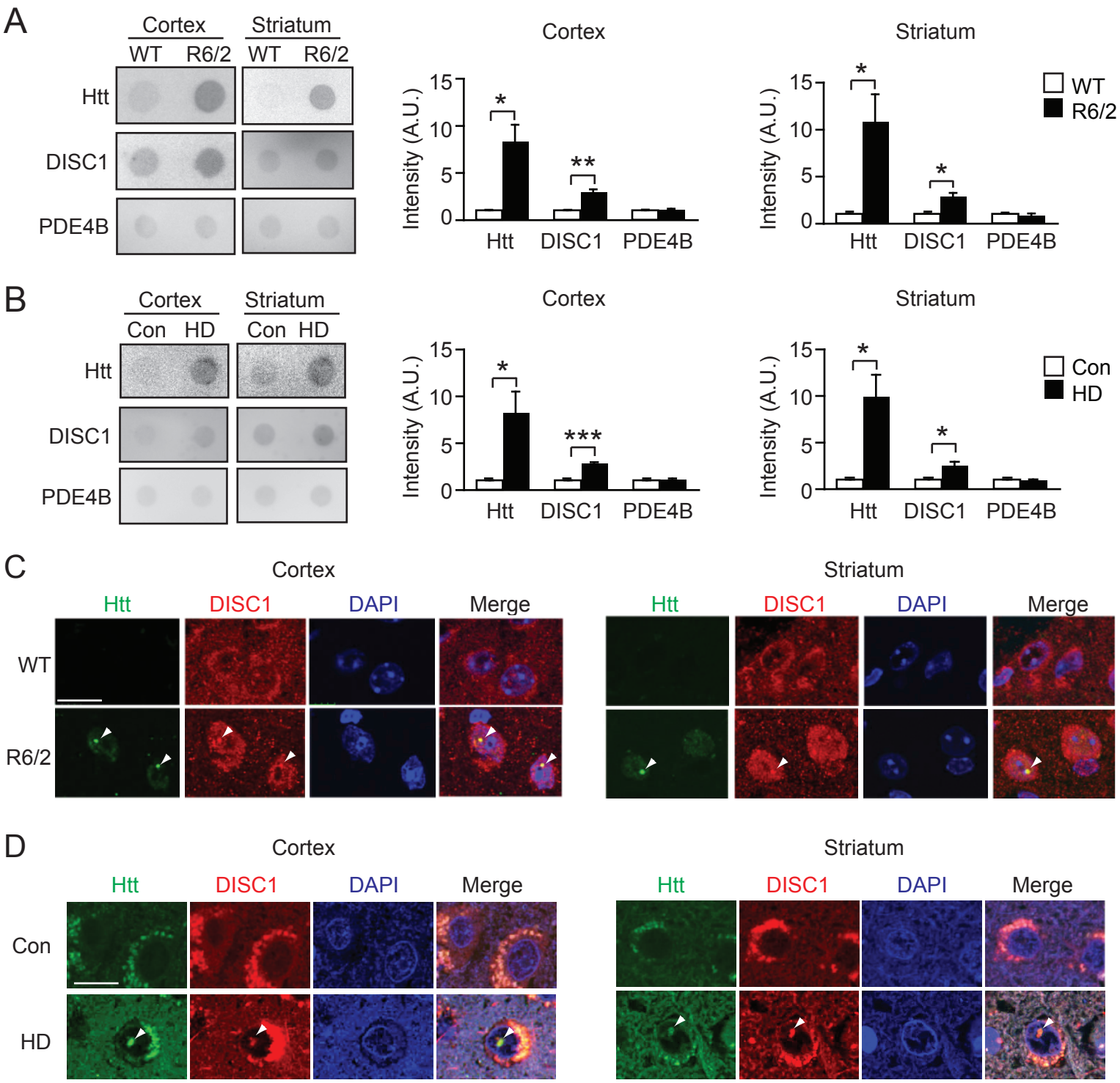

Figure 2. DISC1, but not PDE4B, is sequestered into insoluble Htt aggregates in HD.

(A) Filter trap assay with homogenates of cerebral cortex or striatum from 12-week-old R6/2 mice showed significantly increased levels of Htt (EM48) (top) and DISC1 (mEx3) (middle), but not PDE4B (pan PDE4B) (bottom) in the SDS-resistant fraction, compared with those from wild-type (WT) mice. Error bars denote S.E.M. **P*<0.05, ***P*<0.01.

(B) Filter trap assay with homogenates of cerebral cortex or striatum showed significantly increased levels of Htt (EM48) (top) and DISC1 (h2p) (middle), but not PDE4B (pan PDE4B) (bottom) in the SDS-resistant fraction from HD patients (HD), compared to those from controls (Con). Error bars denote S.E.M. **P*<0.05, ****P*<0.001.

(C) Immunostaining of frozen sections of cerebral cortex (left) or striatum (right) demonstrated that DISC1 was colocalized with intranuclear inclusions of mutant Htt in 12-week-old R6/2 mice. Green, Htt (EM48); red, DISC1 (m317C); blue, DAPI (the nucleus). Arrowheads show intranuclear inclusions. Scale bar, 10 μm.
(D) Immunostaining of paraffin sections of cerebral cortex (left half) or striatum (right half) in HD patients (HD) and human controls (Con) was performed with anti-Htt (EM48) (green, left) and anti-DISC1 (h316C) (red) antibodies. Nucleus was stained by DAPI (blue). Merged images are shown on the right. Arrowheads show intranuclear inclusions. Scale bar, 10 μm.

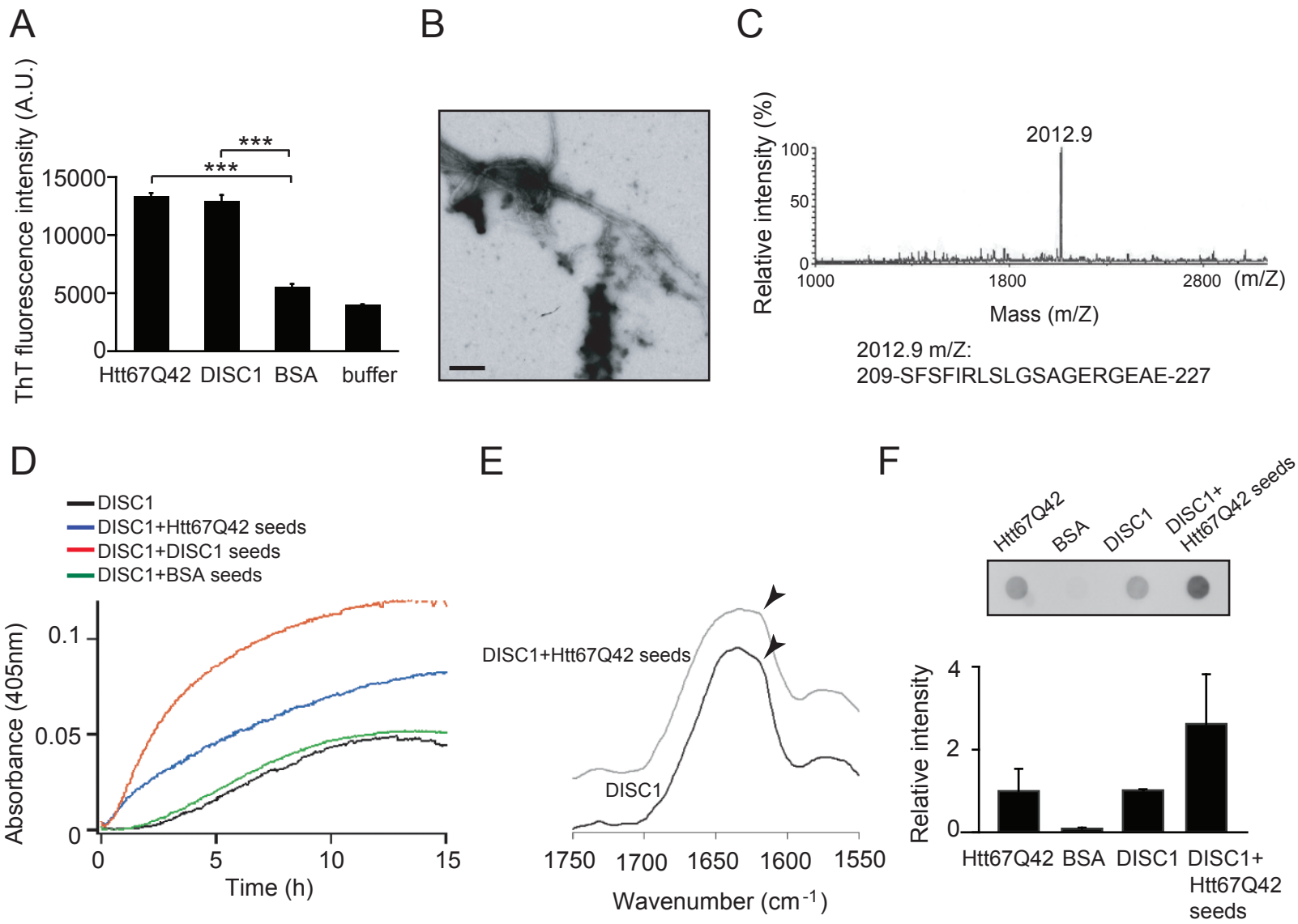

Figure 3. Aggregation of intrinsically amyloidogenic DISC1 is accelerated by cross-seeding with polyQ-expanded mutant Htt.

(A) Thioflavin T (ThT) fluorescent intensities of DISC1 and Htt67Q42 aggregates were significantly higher than that of BSA aggregates. Error bars denote S.E.M. ***P<0.001.
(B) Fibrillar morphology of typical DISC1 amyloid shown by transmission electron microscopy. Scale bar, 100 nm.
(C) MALDI-TOF mass spectrum of DISC1 aggregates digested by proteinase K indentified a major mass peak at 2012.9 m/Z corresponding to residues 209-227 in DISC1 as the core of DISC1 aggregates.
(D) Aggregation of DISC1, which was monitored by the absorbance (turbidity) at 405 nm, was significantly accelerated by the Htt67Q42 aggregate seeds but not by BSA aggregates.
(E) FT-IR spectra revealed that the DISC1 aggregates formed in the presence of Htt67Q42 aggregate seeds (grey) contained more intermolecular β-sheet structures (arrowheads) than did spontaneously formed DISC1 aggregates (black).
(F) The DISC1 aggregates formed in the presence of Htt67Q42 aggregate seeds showed higher resistance to 2% SDS than spontaneously formed DISC1 aggregates in the filter trap assay with Sypro Ruby staining. Error bars denote S.E.M.

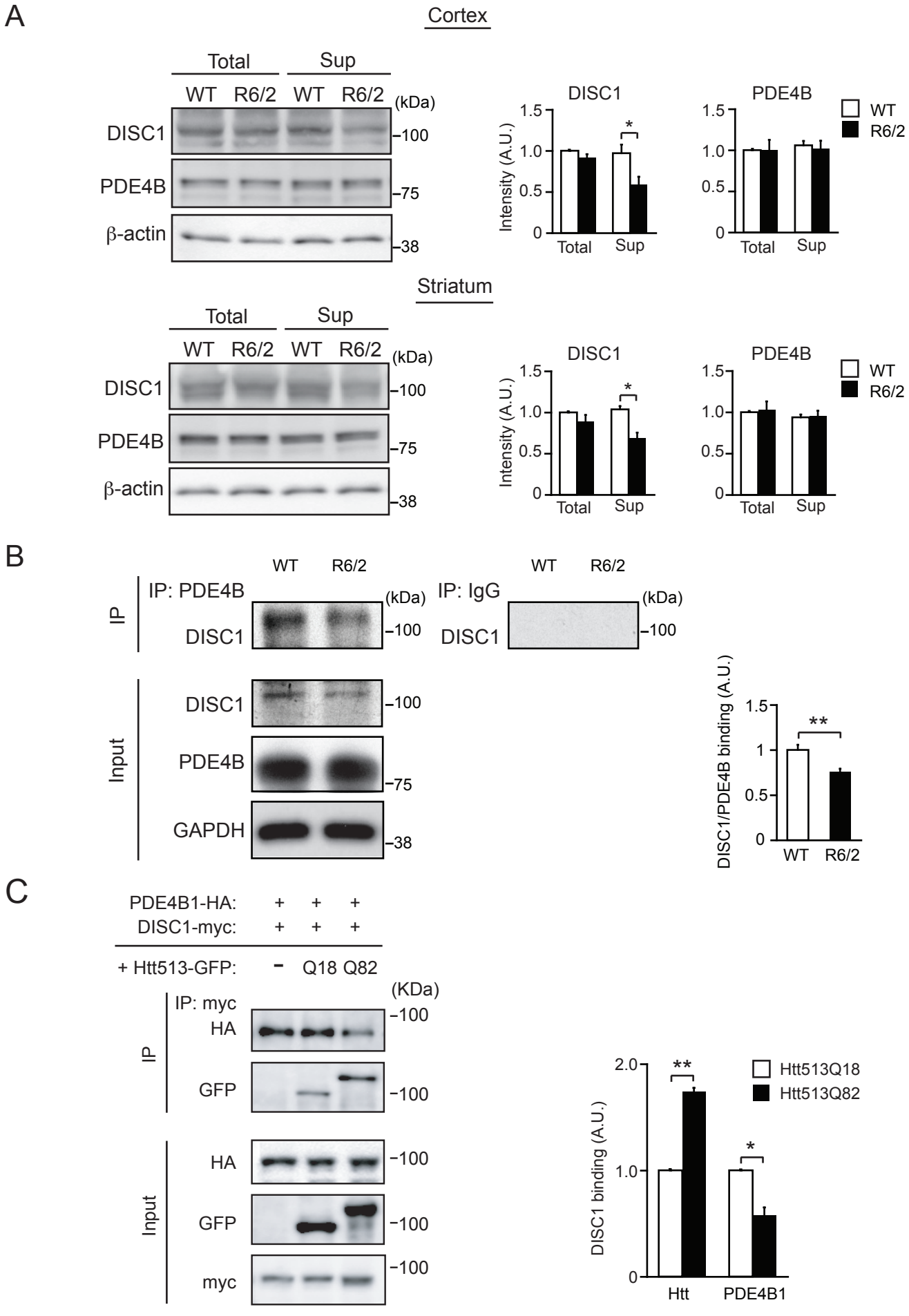

Figure 4. DISC1-PDE4 interactions are reduced by decreased soluble DISC1 levels in the R6/2 mice.

Figure 4

(A) Soluble DISC1, but not soluble PDE4B levels in supernatant fractions (Sup) were reduced in cerebral cortex (top) and striatum (bottom) from 12-week-old R6/2 mice, compared to those from wild-type (WT) mice. Total DISC1 and PDE4B levels in total homogenates (Total) were not changed between WT and R6/2 mice. β-actin is a loading control. DISC1 antibodies (mEx3 for cortex, m317C for striatum) were used for immunblotting. Error bars denote S.E.M. **P*<0.05.
(B) Binding between PDE4B and DISC1 in 12-week-old R6/2 mouse brains was decreased compared to that of wild-type (WT) brains. Immunoprecitation was performed by an anti-pan PDE4B antibody, followed by immunoblotting with anti-DISC1 antibody (D27). Error bars denote S.E.M. ***P*<0.01.
(C) Exogenous addition of Htt513Q82, but not Htt513Q18, significantly reduced DISC1-PDE4B interactions in HEK293T cells. Lysates of the cells overexpressing GFP alone (−), Htt513Q18-GFP (Q18), or Htt513Q82-GFP (Q82) were added to lysates of the cells overexpressing DISC1-myc and PDE4B1-HA. Mixtures were processed for immunoprecipitation with an anti-c-myc antibody, followed by immunoblotting. Error bars denote S.E.M. **P*<0.05, ***P*<0.01.

Figure 5

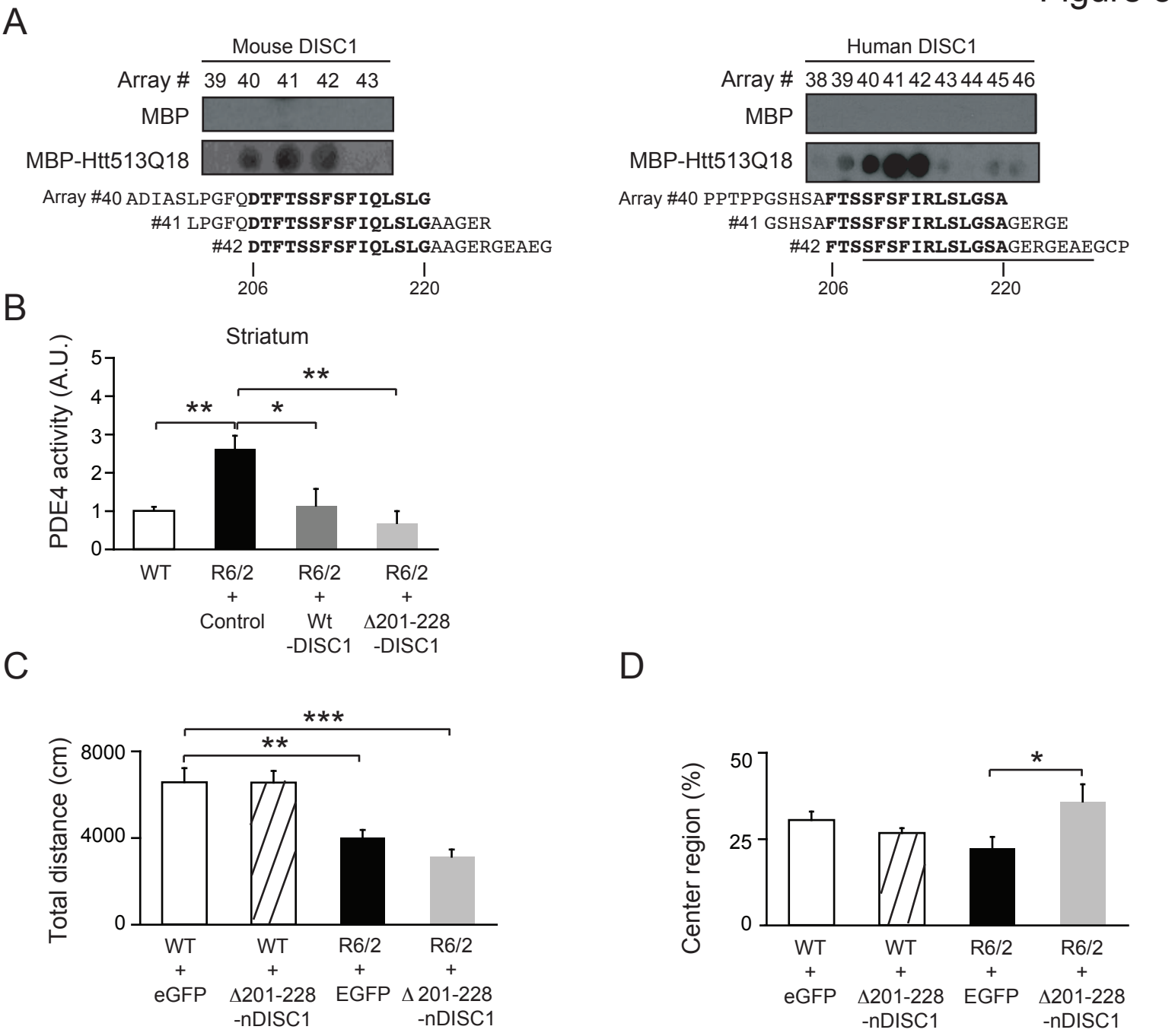

Figure 5. Aberrantly enhanced PDE4 activity and anxiety levels in the R6/2 mice are recovered by exogenous DISC1 expression.

(A) The 25mer-peptides #40-#42 [residues 194-228 for mouse DISC1 (left), residues 196-230 for human DISC1 (right)] in DISC1 showed binding to maltose binding protein (MBP)-Htt513Q18 (bottom) but not MBP alone (top) on peptide array. A black line corresponds to the amyloid core region identified by limited proteolysis and mass spectrometry (see **Figure 3C**).
(B) Aberrant augmentation of PDE4 activity in striatum of R6/2 mice was normalized with Wt or Δ201-228-DISC1. Error bars denote S.E.M. **P*<0.05, ***P*<0.01.
(C) The locomotor activity of R6/2 mice was not affected by expression of Δ201-228-nDISC1. Total distance moved in the open field test was measured in mice at 8 weeks. Error bars denote S.E.M. n=15, 15, 18, 17 for WT+EGFP, WT+Δ201-228-nDISC1, R6/2+EGFP, R6/2+Δ201-228-nDISC1 mice, respectively. ***P*<0.01, ****P*<0.001.
(D) The anxiety levels in R6/2 mice were reduced by expression of Δ201-228-nDISC1. The time spent in a center region in the open field test was measured in mice at 8 weeks. Error bars denote S.E.M. n=15, 15, 18, 17 for WT+EGFP, WT+Δ201-228-nDISC1, R6/2+EGFP, R6/2+Δ201-228-nDISC1 mice, respectively. **P*<0.05.